AGU PUBLICATIONS

JGR

Journal of Geophysical Research: Space Physics

RESEARCH ARTICLE
10.1002/2014JA020024

Key Points:
- Cassini RPWS detects dust impacts as voltage pulses induced on the antennas
- The dust size distribution and density can be inferred from the measurements
- The observed dust density and size distribution are consistent with CDA results

Supporting Information:
- Figures S1–S15
- Text S1

Correspondence to:
S.-Y. Ye,
shengyi-ye@uiowa.edu

Citation:
Ye, S.-Y., D. A. Gurnett, W. S. Kurth, T. F. Averkamp, S. Kempf, H.-W. Hsu, R. Srama, and E. Grün (2014), Properties of dust particles near Saturn inferred from voltage pulses induced by dust impacts on Cassini spacecraft, *J. Geophys. Res. Space Physics*, *119*, 6294–6312, doi:10.1002/2014JA020024.

Received 28 MAR 2014
Accepted 22 JUL 2014
Accepted article online 24 JUL 2014
Published online 15 AUG 2014

Properties of dust particles near Saturn inferred from voltage pulses induced by dust impacts on Cassini spacecraft

S.-Y. Ye[1], D. A. Gurnett[1], W. S. Kurth[1], T. F. Averkamp[1], S. Kempf[2], H.-W. Hsu[2], R. Srama[3,4], and E. Grün[2]

[1]Department of Physics and Astronomy, University of Iowa, Iowa City, Iowa, USA, [2]Laboratory of Atmospheric and Space Physics, University of Colorado Boulder, Boulder, Colorado, USA, [3]IRS, University Stuttgart, Stuttgart, Germany, [4]Center for Astrophysics, Space Physics and Engineering Research (CASPER), Baylor University, Waco, Texas, USA

Abstract The Cassini Radio and Plasma Wave Science (RPWS) instrument can detect dust particles when voltage pulses induced by the dust impacts are observed in the wideband receiver. The size of the voltage pulse is proportional to the mass of the impacting dust particle. For the first time, the dust impacts signals measured by dipole and monopole electric antennas are compared, from which the effective impact area of the spacecraft is estimated to be 4 m^2. In the monopole mode, the polarity of the dust impact signal is determined by the spacecraft potential and the location of the impact (on the spacecraft body or the antenna), which can be used to statistically infer the charge state of the spacecraft. It is shown that the differential number density of the dust particles near Saturn can be characterized as a power law $dn/dr \propto r^{\mu}$, where $\mu \sim -4$ and r is the particle size. No peak is observed in the size distribution, contrary to the narrow size distribution found by previous studies. The RPWS cumulative dust density is compared with the Cosmic Dust Analyzer High Rate Detector measurement. The differences between the two instruments are within the range of uncertainty estimated for RPWS measurement. The RPWS onboard dust recorder and counter data are used to map the dust density and spacecraft charging state within Saturn's magnetosphere.

1. Introduction

The detection of dust particles at Saturn by the radio and plasma wave instruments dated back to Voyager times [*Scarf et al.*, 1982; *Warwick et al.*, 1982; *Gurnett et al.*, 1983]. The Radio and Plasma Wave Science (RPWS) experiment onboard Cassini is equipped with a more sophisticated set of antennas and receivers than Voyager [*Gurnett et al.*, 2004]. So it can provide more information on the dusty plasma environment near Saturn and the numerous Cassini orbits provide a much larger coverage compared to the two Voyager flybys. The waveform captured by the wideband receiver (WBR) provides an excellent way to record individual dust impacts. During the Cassini Saturn Orbit Insertion (SOI) and many E ring crossings, RPWS has demonstrated the ability to measure dust particles in the Saturn system via voltage pulses induced by the dust impacts on the spacecraft [*Wang et al.*, 2006; *Kurth et al.*, 2006]. Besides, the voltage spectrum on the monopole electric antenna analyzed by the low-resolution receivers can be used to estimate the average size/mass of the dust grains [*Aubier et al.*, 1983; *Meyer-Vernet*, 1985; *Meyer-Vernet et al.*, 1986]. This technique of dust detection, very similar to those used on the Voyager plasma wave and radio astronomy instruments, is expected to complement the measurements from Cassini's Cosmic Dust Analyzer (CDA).

Although CDA is a specially designed, dedicated dust instrument, RPWS has a much larger collecting area than the aperture of CDA, so RPWS is expected to be able to detect much lower fluxes. More importantly, the RPWS does not need a specific spacecraft attitude for dust detection, so it is possible for RPWS to detect dust continuously through the orbit. During SOI, a one-time passage, RPWS provided the only measurement of dust particles in this crucial region [*Wang et al.*, 2006], whereas CDA was not operating due to the spacecraft pointing constraints. On the other hand, the design and calibration of the CDA [*Srama et al.*, 2004] enables a more accurate determination of grain mass, velocity, charge, direction of arrival, and even elemental composition, provided an appropriate spacecraft attitude. In section 4, the RPWS result will be compared with the CDA result to show that the data from the two instruments are generally consistent with each other.

In this paper, we apply a new dust detection algorithm to the WBR data, which improves the detection of dust impacts and differentiates the impacts from plasma wave interferences. We compare for the first time the

waveforms of dust impacts measured by monopole and dipole antennas, which leads to a clarification of the difference in the detection mechanisms of these two modes. An estimation of the effective impact area of the spacecraft is derived based on the statistical analysis of the polarities of the impacts.

Saturn's tenuous E ring is the largest ring in the solar system and extends from about 3 Rs to at least 8 Rs [*Nicholson et al*., 1996]. The E ring particles were first directly detected by the Pioneer 11 and the Voyager 1 spacecraft [*Humes et al*., 1980; *Tsintikidis et al*., 1995; *Meyer-Vernet et al*., 1996]. Cassini provides a great opportunity for in situ studies of the dust particles in the E ring with both CDA and RPWS experiments. After Cassini's SOI in July 2004, the spacecraft has made a number of crossings of the E ring, near the orbit of Enceladus. *Kurth et al*. [2006] reported the characteristics of the E ring particles and dust density profile, which are generally in agreement with CDA observations [*Kempf et al*., 2008], the empirical model given by *Showalter et al*. [1991], and the dynamical model by *Juhasz and Horanyi* [2002], *Juhasz et al*. [2007], and *Horanyi et al*. [2008]. We reanalyze of the waveform data captured by RPWS WBR during the E ring crossings and recalculate the particle sizes based on a new impact mass-to-charge yield.

One of the most spectacular discoveries of the Cassini mission was the plume of water vapor and icy particles (dust) originating near the south pole of Saturn's moon Enceladus [*Dougherty et al*., 2006; *Porco et al*., 2006]. This plume consists of both water group neutrals [*Waite et al*., 2006] and water ice particles (dust) [*Spahn et al*., 2006]. The water group neutrals and ice particles ejected by the moon constitute the major content of the E ring and the Enceladus torus, and after ionization the neutrals become a major source of plasma in Saturn's magnetosphere.

Both RPWS and CDA are sensitive to micron size dust particles near Enceladus [*Srama et al*., 2006; *Kempf et al*., 2008; *Farrell et al*., 2009, 2010; *Omidi et al*., 2012]. Nanometer-sized particles inside the Enceladus plume are detected by the Cassini Plasma Spectrometer (CAPS) experiment, where nanograins appear as high-energy charged particles in the electron (ELS) and ion mass spectrometers [*Jones et al*., 2009; *Hill et al*., 2012]. The submicron dust particles, through trapping of electrons, are mainly responsible for the large difference between the ion and electron densities in the vicinity of Enceladus as measured by the Langmuir probe [*Wahlund et al*., 2009; *Yaroshenko et al*., 2009; *Shafiq et al*., 2011; *Morooka et al*., 2011]. Based on the analysis of the WBR data, we derive the size distribution and density of micrometer-sized dust particles inside the plume, which will be important inputs for future modeling studies.

From 2005 to 2013, Cassini has made 20 flybys of Enceladus and during some of the flybys flew through the plume. RPWS provides measurements of dust properties (size distribution and density) during all these flybys. These measurements provide important information for the density profile and possible variability in the source rate of the Enceladus plume [*Saur et al*., 2008; *Kempf et al*., 2010; *Smith et al*., 2010; *Dong et al*., 2011]. Based on the size distribution and density of micron-sized dust and nanoparticles, one can model the distribution of the tens of nanometer-sized particles, which was only constrained by Langmuir probe measurements [*Morooka et al*., 2011; *Shafiq et al*., 2011; *Dong and Hill*, 2013].

2. Instrumentation

This study involves two experiments onboard Cassini that are sensitive to the dust particles. The CDA is a specially designed, dedicated dust instrument. The RPWS can detect dust impacts via the voltage waveform and power spectrum measured on the electric antennas. The RPWS-Langmuir probe can infer the dust population through the discrepancy of the ion and electron density and the slowdown of the ions near the Enceladus orbit through measurements of plasma inhomogeneities (dn/n) induced by the charged grains [*Wahlund et al*., 2009].

2.1. RPWS

The Cassini Radio and Plasma Wave Science (RPWS) instrument measures oscillating electric fields over the frequency range 1 Hz to 16 MHz and magnetic fields in the range 1 Hz to 12 kHz [*Gurnett et al*., 2004]. The instrument uses three nearly orthogonal electric field antennas (E_u, E_v, and E_w) and three orthogonal magnetic search coil antennas, providing a direction-finding capability. E_u and E_v antennas are often used together as the E_x dipole antenna and E_w as a monopole antenna.

There are five receiver systems in the RPWS instrument, only one of which is involved in this study, the high-resolution WBR that covers two frequency bands, 60 Hz to 10.5 kHz and 800 Hz to 75 kHz. The WBR

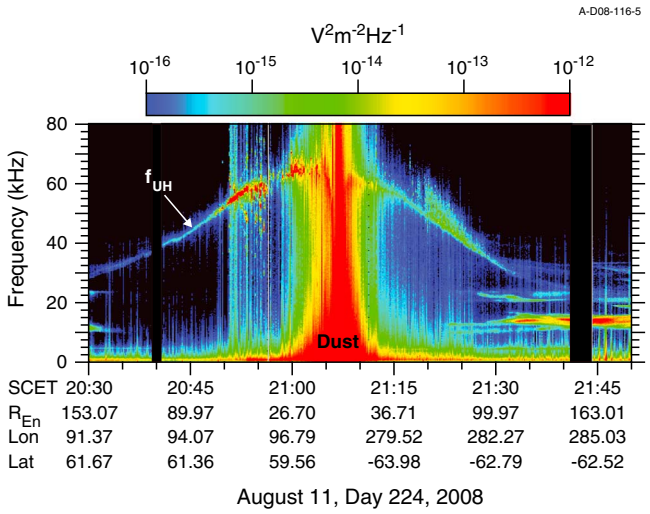

Figure 1. WBR spectrogram of E4 flyby shows wave power as a function of frequency and time. Dust impacts are identified as broadband bursts extending well above the local plasma frequency (indicated by the upper hybrid resonance).

records waveform snapshots of voltages measured on the RPWS antennas (either monopole or dipole), which can be Fourier transformed to provide high-resolution spectra of low-frequency radio/plasma waves and dust impact signatures. Due to the 8 bit dynamic range of the WBR, the gain of the receiver is automatically selected from 0 to 70 dB at 10 dB steps to accommodate signals induced by plasma waves and dust impacts. Figure 1 shows a high-resolution frequency-time spectrogram of WBR (connected to the E_x dipole antenna in the 80 kHz mode) data during the E4 flyby. The dust impacts can be identified as intense broadband burst structures which extend well above the upper hybrid resonance. The broadband nature of the impact spectrum is a direct consequence of Fourier transforming a short impulsive waveform. The WBR also serves as the front end for the onboard dust detection function, which provides two kinds of data: waveform snapshot of dust impact and dust counts, when the WBR is not scheduled to record high-resolution data.

2.2. RPWS-Langmuir Probe

The RPWS-Langmuir probe is designed to provide in situ information of the ambient plasma, i.e., the electron/ion density and temperature [*Gurnett et al*., 2004; *Wahlund et al*., 2005]. This is achieved by varying the bias potential applied to the Langmuir probe and analyzing the resulting current. Another key parameter that can be measured by the Langmuir probe is the spacecraft floating potential, which can be used as a proxy for the potential of the dust particles. In a hot tenuous plasma, the sunlit spacecraft emits photo electrons to balance the current from the electrons of the ambient plasma, so the potential of the spacecraft is generally positive. In cold dense plasma, the electron current is larger than the ion current due to the electrons' higher thermal velocity, so the spacecraft is normally charged negatively.

2.3. CDA

The Cosmic Dust Analyzer (CDA) has two subsystems, the High Rate Detector (HRD) and the Dust Analyzer (DA) [*Srama et al*., 2004]. There are two sensors in HRD with different collecting areas (M sensor: 50 cm^2, m sensor: 10 cm^2) [*Kempf et al*., 2008]. The sensors uses thin polarized foils for the dust detection and can measure high impact rates of particles bigger than about 800 nm at 8 km/s impact velocity. The detection thresholds of the thin foils depend on the ram speed of the spacecraft, so the threshold is around 500 nm for higher impact speed (~11 km/s). The impact rates measured with different sensing foils (corresponding to different size thresholds) can be used to infer the slope of the size distribution function. Based on impact ionization, the DA measures the electric charge carried by dust particles, impact direction, ram velocity, mass, and elemental composition. The potential of the dust grains can be derived from DA measurements.

3. RPWS Dust Detection Mechanism

3.1. Impact Ionization

Impact ionization is believed to be the basis for various proposed mechanisms for converting the impact energy to an electrical signal [*Gurnett et al*., 1983, 1987, 1991; *Meyer-Vernet*, 1985]. When a dust particle strikes the spacecraft with very high velocity, kinetic energy in the collisions vaporizes the particle and part of the target material. This results in a hot ionized gas with electrons expanding away from the impact site

faster than ions. The charge Q in the expanding plasma cloud depends on the mass and velocity of the impacting dust grain.

Experiments have been carried out to measure the charge yield of iron particles impacting the surface materials (RPWS electric antenna, Kapton blanket, and black Polyimide) of the Cassini spacecraft (Grün, Pawlinka, and Srama, MPI, unpublished result; see the supporting information). The measured charge yield for iron particles impacting on Kapton is

$$Q/m = 0.01 \times v^{4.6} \tag{1}$$

where Q is expressed in Coulombs, m in kilograms, and v in km/s.

The charge yield factor varies by over an order of magnitude across different experimental studies [*Adams and Smith*, 1971; *Dietzel et al*., 1973; *Göller and Grün*, 1989; *McBride and McDonnell*, 1999]. For example, the charge yield factor 0.4 C/g used by *Wang et al*. [2006] for the SOI (16 km/s impact velocity) dust impacts is about 10 times smaller than equation (1). The exponent of mass in equation (1) could be smaller than 1 if recombination and surface phenomenon play an important role, which should occur for very large grains [*Krüger and Kissel*, 1984]. The exponent of the velocity is a function of impact velocity and could range from 2.5 to 5.5 [*Dietzel et al*., 1973; *Krüger and Kissel*, 1984]. The exponent of velocity is 3.5 in the charge yield equations used by *Pedersen et al*. [1991] and *Meyer-Vernet et al*. [1996] for Voyager dust impacts. Collette et al. carried out experiments measuring the impact plasma yield using different target materials commonly used on spacecraft (A. Collette et al., Micrometeoroid impact-charge yield for common spacecraft materials, unpublished; see the supporting information). They showed that for all common materials used on spacecraft the variability in the impact charge yield is small. The charge yield coefficient can be approximated as $Q/m = 55$ C/kg for 10 km/s impact velocity, about 7 times smaller than equation (1). Note that the yield of ice particles impacting on Kapton could be lower than equation (1). Impact experiment using ice target showed 100 times lower yield than metal target [*Timmermann and Grün*, 1991]. It is believed that the charge yield does not change significantly when target and projectile materials are interchanged. However, the charge yield will increase significantly once there are salts in the ice matrix, which is the case for some fraction of the E ring population. The uncertainty in the charge yield will translate into uncertainty in the mass of the ice grains calculated from the magnitude of the impact voltage pulses.

3.2. Generation of Voltage Pulse

Oberc [1996] summarized the possible ways for the electric charge generated by a dust impact to induce a potential difference between the antenna and the spacecraft body: (1) The spacecraft body recollects impact charges; (2) The antenna recollects impact charges; and (3) The antenna senses the electric field created by the charge separation inside the expanding plasma cloud. For Scenarios (1) and (2), the spacecraft potential determines whether electrons or ions will be recollected by the spacecraft body or the antenna. Inside the E ring, Cassini is generally negatively charged, so the ions from the impact plasma cloud will be recollected. For Scenarios (2) and (3), the signal levels generated in the WBR by the impact charges depend on the impact location. The choice of antenna mode (monopole or dipole) will also have a significant impact on the efficiency of change collection and the resulting voltage signal level.

For the monopole mode, recollection of impact charges by the spacecraft body is responsible for the voltage pulses detected. The size of the voltage pulse measured in the receiver is proportional to the charge recollected by the spacecraft body,

$$V = \alpha\beta Q/C \tag{2}$$

where $C = 200$ pF is the capacitance of the Cassini spacecraft body [*Wang et al*., 2006] and $\beta = \frac{C_A}{C_A + C_B} \approx 0.4$ is a factor that takes into account the voltage reduction due to the known base capacity of the antenna [*Gurnett*, 1998; *Gurnett et al*., 2004]. The charge collection coefficient is α which could range from 0 to 1 for the charge-spacecraft coupling in the monopole mode. If a dust particle directly impacts the electric antenna, recollection of impact charges by the antenna is responsible for the voltage pulse. In that case, the capacitance in equation (2) needs to be replaced by the capacitance of the electric antenna $C_A = 100$ pF.

For the dipole mode, *Gurnett et al*. [1987] proposed recollection of impact charges by one of the electric antenna near the impact site to interpret the dust impact signals. This is supported by laboratory experiments and simulation study. *Sheehan et al*. [1995] in an experiment demonstrated the expanding

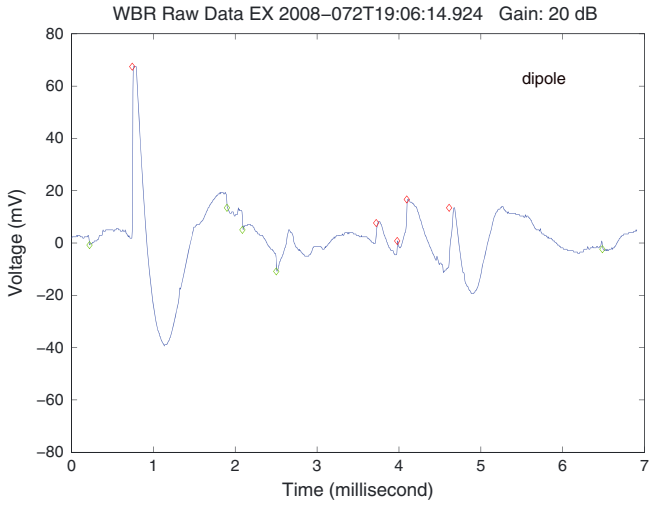

Figure 2. Sample WBR waveform snapshot (80 kHz mode, E_x dipole antenna) showing dust impact signatures detected during the E3 flyby. The dust impacts are identified by red (positive pulse)/green (negative pulse) diamond markers.

plasma cloud can induce a voltage pulse on the dipole antenna similar to that observed by the Voyager plasma wave instruments. They showed that the delay time of the voltage pulses is proportional to the distance between the origin of the expanding plasma and the antenna, indicating that voltage signal is caused by the recollection of the escaping charges. *Lee et al*. [2012, 2013] in their laboratory experiments showed that impact-generated ions with different masses were detected by the charge collector at different delay times. *Pantellini et al*. [2012a] simulated the interaction between the expanding impact plasma cloud with an electric antenna and concluded that the electrostatic potential difference between the cloud's center and infinity predicted by the model is far too weak to account for the voltage pulses observed on the STEREO S/WAVES time domain sampler following a nanosized dust particle impact.

In the dipole mode, the charge recollection efficiency is greatly reduced due to the smaller collecting area of the electric antenna compared to the spacecraft body. This is partly responsible for the smaller voltage spectral power of dust impacts observed by the dipole antenna compared to the monopole antenna [*Meyer-Vernet et al*., 2009]. The studies on the Voyager plasma wave science (PWS) detections of dust impacts concluded that the α coefficient for charge-antenna coupling in the dipole mode is ~100 times smaller than that for the monopole mode [*Gurnett et al*., 1983, 1987; *Tsintikidis et al*., 1994]. The 100 factor probably include the effect of the common mode rejection, which would attenuate similar signals on the $+x$ and $-x$ elements of the dipole antenna by ~20 dB. This discrepancy between the dipole and monopole measurements will be further discussed.

4. RPWS WBR Waveform Data Analysis

4.1. Waveform Inspection and Dust Impact Identification Algorithm

The waveforms recorded by the RPWS WBR provide an excellent way of registering dust impacts on the spacecraft. The dust impact waveforms typically exhibit a very rapid rise on a timescale of a few tens of microseconds, followed by a complicated recovery waveform. Figure 2 shows an example of WBR waveform snapshot (80 kHz mode, E_x dipole antenna) where dust impacts are marked by diamonds at the peak of each voltage impulse. A dust impact is characterized as a sudden jump in the differential voltage. To identify the dust impacts, the voltage changes between each two adjacent data points are calculated. If at any time the voltage change exceeds a threshold value (for example, 4 times the voltage change averaged over the previous 15 data points), a dust impact is registered. Once a dust impact is identified, the jump in data number is recorded, which is then converted to the magnitude of the voltage jump, taking into account of the gain of the receiver. The voltage conversion formula is given by

$$V = \sqrt{2}p/cg \tag{3}$$

where V is the peak size in Volts with its sign indicating the polarity of the pulse, p is the jump in data number, c is a calibration factor (267.31 for 80 kHz mode and 264.25 for 10 kHz mode), and $g = 10^{dB/20}$ is the receiver voltage gain.

This algorithm is designed based on the algorithm used by *Wang et al*. [2006] and *Kurth et al*. [2006]. The new algorithm has several advantages: (1) It detects more and smaller dust impacts; (2) There is no need to adjust the threshold for different WBR gain levels; and (3) It can effectively distinguish dust impacts from the

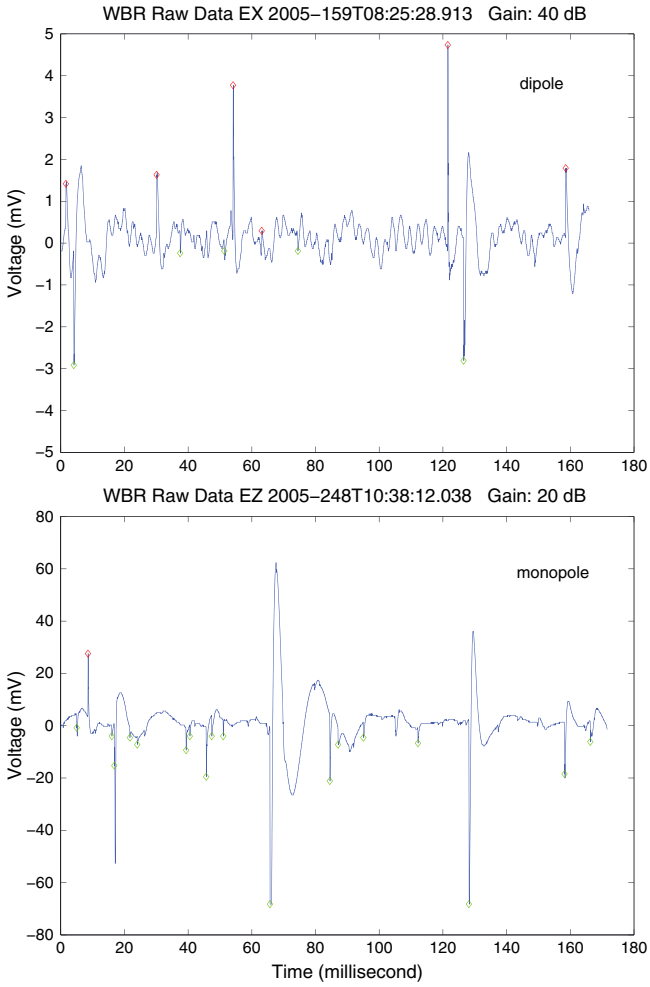

Figure 3. Comparison of waveform snapshots of RPWS WBR (10 kHz mode) showing dust impact signatures observed with (top) the E_x dipole antenna and (bottom) the E_w monopole antenna.

interference of plasma waves. Although one would expect the slope of the voltage pulses to be different for 10 kHz and 80 kHz modes, the same algorithm applies to data captured in both modes, because the thresholds for the identification of dust impacts are relative (4 times the average background slopes).

4.2. Comparison of Dipole and Monopole Antenna Measurements

Figure 3 compares the dipole and monopole antenna measurements of dust impacts by the WBR. Figure 3 (top) is a snapshot of a waveform measured by the E_x dipole antenna during the E ring crossing on day of year (DOY) 159, 2005. Figure 3 (bottom) shows the measurements using the E_w monopole antenna during the ring plane crossing at around 3 R_S on DOY 248, 2005. Notice that in the dipole mode, approximately equal numbers of positive and negative voltage pulses were detected. The polarity of the voltage pulses is determined by which electric antenna element is closer to the impact site [*Malaspina et al.*, 2014]. The antenna element closer to the impact site will collect charges from the impact plasma cloud first, resulting in voltage pulse in one polarity. The other antenna element will also collect charges once it is immersed in the impact plasma cloud, causing a reversal of the voltage polarity. In contrast to the dipole observation, mostly negative pulses were observed in the monopole data. The negative pulse is a result of rising spacecraft potential due to the collection of ions from the impact charges, because the spacecraft potential is generally −1 V to −5 V in the E ring [*Wahlund et al.*, 2005; *Sittler et al.*, 2006; *Morooka et al.*, 2011; *Hsu et al.*, 2012, 2013]. The Langmuir probe measured spacecraft potential was all negative during 08:00–13:00, about −4.7 V at 8:00, increasing to −2.0 V around 10:00 (−2.0 V at 10:39:38.91), and decreasing to −3.5 V at 12:36 on DOY 248, 2005 (M. Morooka, private communication, 2014). In this configuration, the reversal of the voltage after the initial pulse could be due to the collection of escaping ions by the monopole antenna element (some of the ions are energetic enough to escape the negative potential of the spacecraft body). The positive voltage pulse is interpreted as a direct impact on the electric antenna. In this case, the antenna collects the ions from the impact plasma cloud, leading to a rise of the antenna potential.

Figure 4 shows the voltage polarity ratios of the dust impacts detected by the dipole antenna and the monopole antenna during the ring plane crossings on DOY 159, 2005 (left) and DOY 248, 2005 (right), respectively. For the dipole antenna data, the polarity ratio is approximately 1 and slightly modulated by the changing attitude of the spacecraft, shown by the changing angles between the length of the antennas and the ram velocity. This behavior is expected for dust impacts distributed stochastically on the surface of the spacecraft. For the monopole antenna measurement, the ratio of positive/negative pulses detected is approximately 0.05. This ratio could be used to estimate the effective area of the spacecraft based on the interpretation that the negative pulses are impacts on the spacecraft body and the positive pulses are impact on the monopole antenna. The

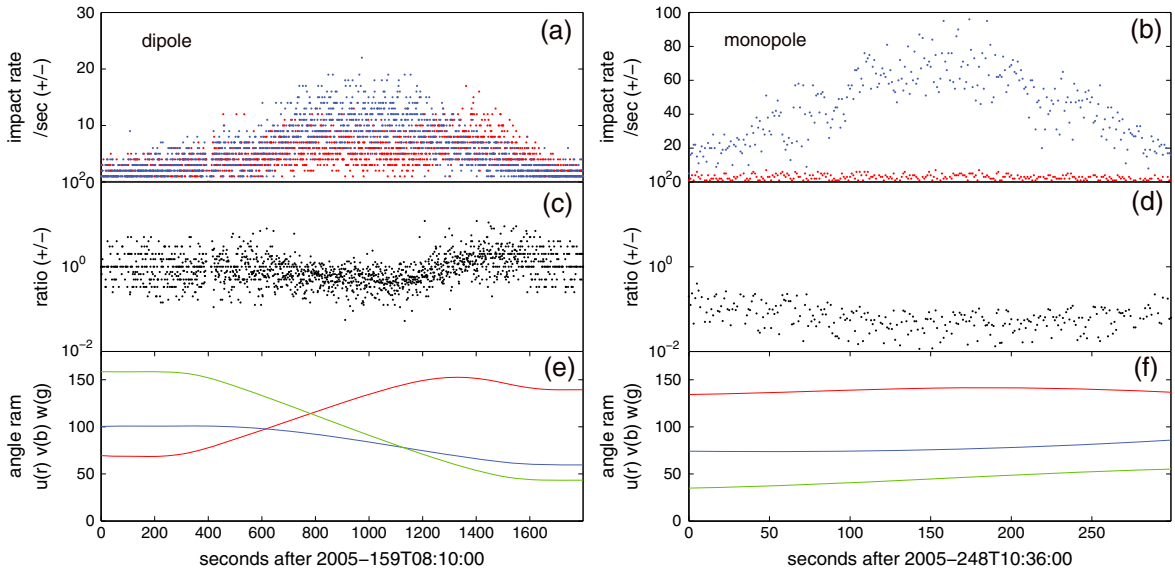

Figure 4. Polarity ratios of the voltage pulses detected during the ring plane crossings on DOY 159, 2005 and DOY 248, 2005. (left) Dipole and (right) monopole antennas were used for dust detection during these two crossings, respectively. (a, b) Red dots indicate the count rates of the positive impacts, while blue dots indicate the count rates of the negative impacts. (c, d) The polarity ratios of the voltage pulses recorded by the dipole and monopole antennas. (e and f) The angles between the ram direction and the length of E_u (red), E_v (blue), and E_w (green) antenna elements.

green line shows the angle between ram direction and the length of the E_w antenna was around 45°. The projected cross-sectional area of the E_w antenna itself is ~0.2 m^2. If all of this projected area is effective for dust impacts, the effective area of the spacecraft body is ~4 m^2 based on the polarity ratio of the monopole measurement. This effective area applies to the monopole antenna measurements. For the dipole mode, the effective area might be smaller because dust impacts that are symmetric to the dipole antenna would be hard to detect due to the common mode rejection. This calculation constrains the value of the effective area, which has direct impact on the uncertainty when calculating dust densities from impact rates [*Kurth et al.*, 2006].

Figure 5 compares the dust detections using the dipole antenna and the monopole antenna during two ring plane crossings on DOY 159, 2005 (4 R_S) and DOY 248, 2005 (3 R_S). The two ring plane crossings have similar impact velocities, 8.2 km/s. Figure 5 (top) shows that the electric field spectral power caused by dust impacts on the monopole and dipole antenna differ by more than 30 dB. Figure 5 (bottom) shows the distribution of the magnitude of the dust impact voltage pulses, which differ by an order of magnitude. Meanwhile, the slopes of the voltage distributions are both around −2. The dipole antenna detected ~10 times fewer impacts than the monopole antenna (both distributions represent 1 min of data). Note that the dust density at the peak of the E ring near 3.95 R_S at Enceladus' orbit should be higher than at 3 R_S [*Kurth et al.*, 2006, Figure 5]. So the difference in the counts of dust impacts between the two antennas would be even greater if the monopole data were collected at the same location.

Figure 6 shows a waveform snapshot of WBR during a slower (5.6 km/s) ring plane crossing at 3 R_S using the dipole antenna. The dipole antenna detected much fewer dust impacts compared to the monopole measurement at a similar radial distance shown in Figure 3 (bottom). The lower dust count rate shown in Figure 6 is consistent with the expectation and is most likely caused by the dipole configuration and the lower impact speed, both increase the detection mass threshold (there are fewer large particles).

4.3. Mass/Size Distribution

Since the amplitude of the voltage pulse is believed to be proportional to the mass of the impacting particles [*Gurnett et al.*, 1983; *Aubier et al.*, 1983], the mass distribution of the dust particles can be determined from the magnitude distribution of the voltage pulses on the antenna using the Kapton charge yield and equation (2),

$$m \cong \frac{VC}{\alpha\beta 0.01 v^{4.6}}. \quad (4)$$

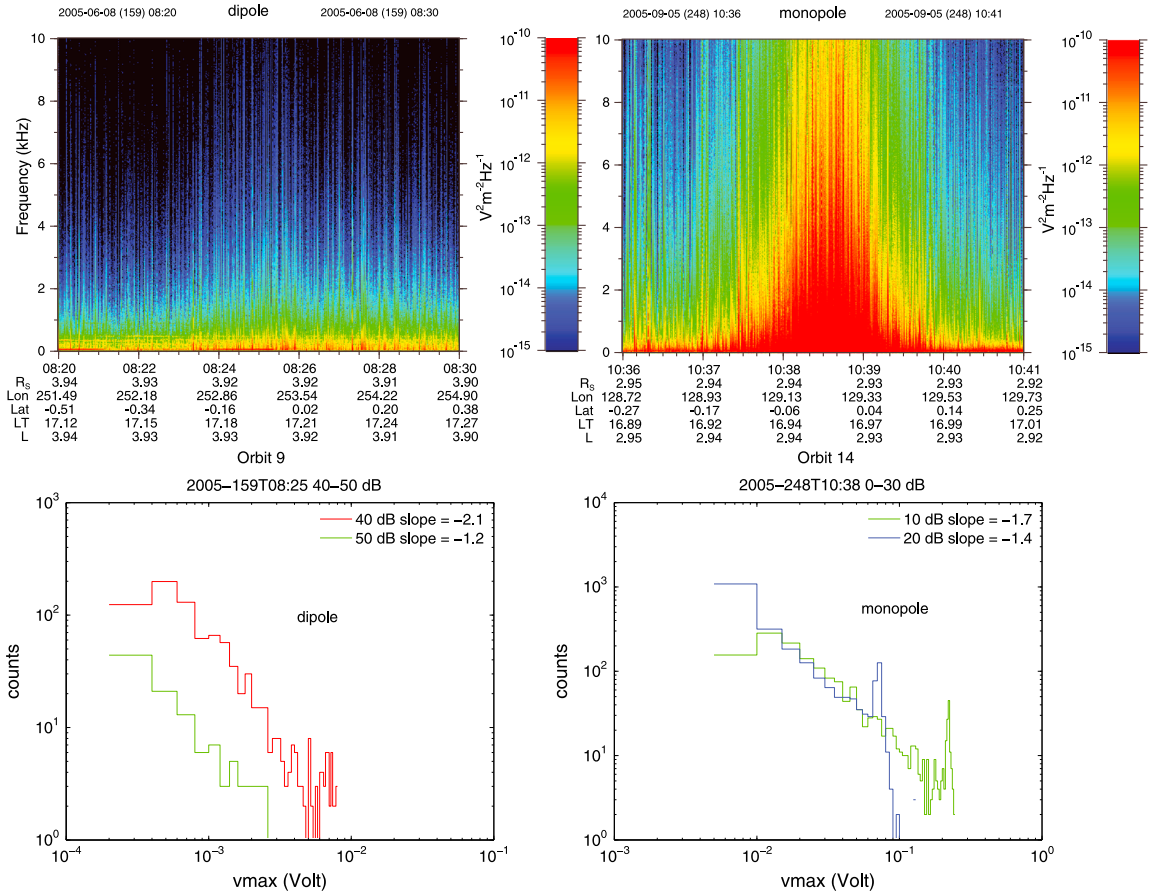

Figure 5. Comparison of (left) the dipole antenna measurement on DOY 159, 2005 and (right) the monopole antenna measurement on DOY 248, 2005. (top) The electric field spectral power and (bottom) the distribution of the magnitude of voltage pulses induced by dust impacts. The ram velocities for these two crossings are both around 8.2 km/s.

In this study, we assume a charge collection efficiency $\alpha = 0.5$ for the monopole mode. For the dipole mode, the voltage jump values are multiplied by a correction factor 40 to account for the less efficient charge collection and the signal attenuation due to the common mode rejection. This correction would make the mass of the dust particles calculated from the dipole mode measurements consistent with those from the monopole mode measurements. Assuming a spherical shape for the ice grains and knowing the density of water ice $\rho = 0.92 \times 10^3$ kg/m^3, we can calculate the radius of the dust grains with

$$r = \left(\frac{3m}{4\pi\rho}\right)^{\frac{1}{3}}. \tag{5}$$

Figure 7 shows the size (radius) calculated from the dipole and monopole mode measurements during the ring plane crossings on DOY 159, 2005 and DOY 248, 2005. The dipole voltage jump was multiplied by the correction factor 40 before the size conversion. It is shown that the dipole and monopole antennas detected similar size particles ($<$10 μm) during these two ring plane crossings, with the dipole antenna less sensitive to smaller dust particles. The size distributions are characterized by a power law distribution with the slope around −4 near Enceladus' orbit and −3 for the ring plane crossing near 3 R_S. Note that in the size distributions there is a decrease toward smaller sizes, probably due to lower sensitivity to dust impacts near the detection threshold. For these two ring plane crossings, the dust detection mechanism is sensitive to dust particles as small as 2–3 μm.

Figure 8 shows the statistics of the dust impact voltage jumps recorded by the WBR during E3, a high inclination flyby of Enceladus. During the 14 min shown in the figure, the gain of WBR ranged from 0 to 60 dB. These gains are automatically selected by the receiver to accommodate signals induced by plasma waves

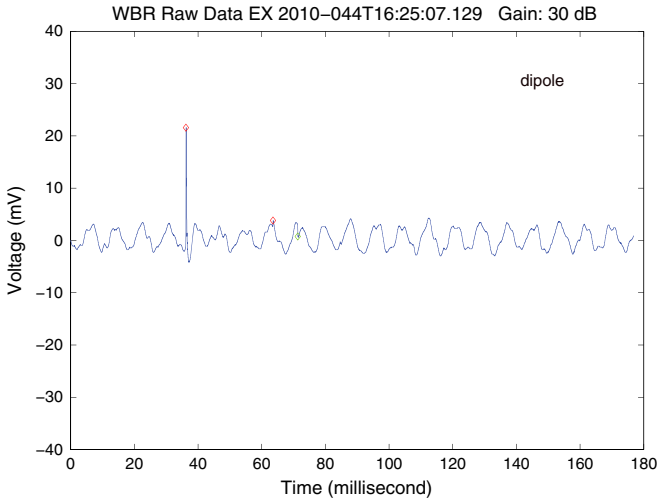

Figure 6. Snapshot of WBR showing dipole antenna detection of dust impacts during the ring plane crossing (3 R_S) on DOY 044, 2010. Much fewer dust impacts were recorded compared to the similar ring plane crossing on DOY 248, 2005 (Figure 3, bottom), where the monopole antenna was used. The dust-spacecraft ram velocity is 5.6 km/s.

and dust impacts, due to the 8 bit dynamic range of the WBR. Larger dust particles impact the spacecraft more frequently near the center of the plume, so the gain is automatically turned down to avoid clipping of the signals. But as a result, it will be harder to detect smaller dust impacts. Figure 8 (middle) shows the number of dust impacts as a function of impact voltage jump size and time. It is shown that at any time, fewer large voltage pulses were detected than small voltage pulses, indicating a power law-like distribution. Figure 8 (bottom) shows the gain of the WBR versus time, which is inversely correlated with the size range of detectable dust particles.

Figure 9 shows the differential size distribution of dust particles detected by the WBR during the E5 flyby. The dust impacts recorded at each gain are sorted into size bins of constant increment to get a differential size distribution function of the dust particles in the plume. The dust impacts detected at different gains are separated because the WBR is sensitive to different size ranges of dust particles at different gains. Similar size distribution slopes around −4 are observed for dust impacts detected at different gains, which indicates that the slope does not change with location. The same slope of −4 in the dust size distribution has been observed during the SOI and E ring crossings. The fitted slopes of the distribution functions are also consistent with the CDA HRD result [*Kempf et al.*, 2008]. The power law size distribution of ice grains at Enceladus is similar to the size distribution of interplanetary dusts detected at 1 AU, where the cumulative flux of dust particles decreases as 1/*m* (*m* is mass of the micrometeoroid) [*Grün et al.*, 1985].

4.4. Impact Rate and Density

The impact rate is calculated by dividing the number of dust impacts within each waveform snapshot with the total time duration of the snapshot. There are usually four (two) snapshots per second in the 80 (10) kHz mode of WBR and each snapshot lasts about 7 (200) ms. These impact rates are then averaged with a 5 s

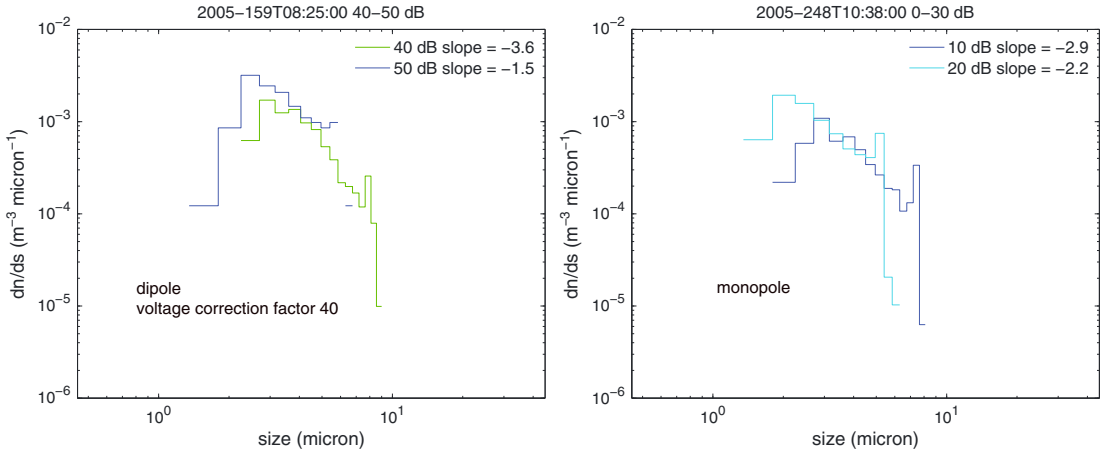

Figure 7. Differential size distribution of dust grains calculated from the dipole and monopole measurements during the ring plane crossings on (left) DOY 159, 2005 and (right) DOY 248, 2005.

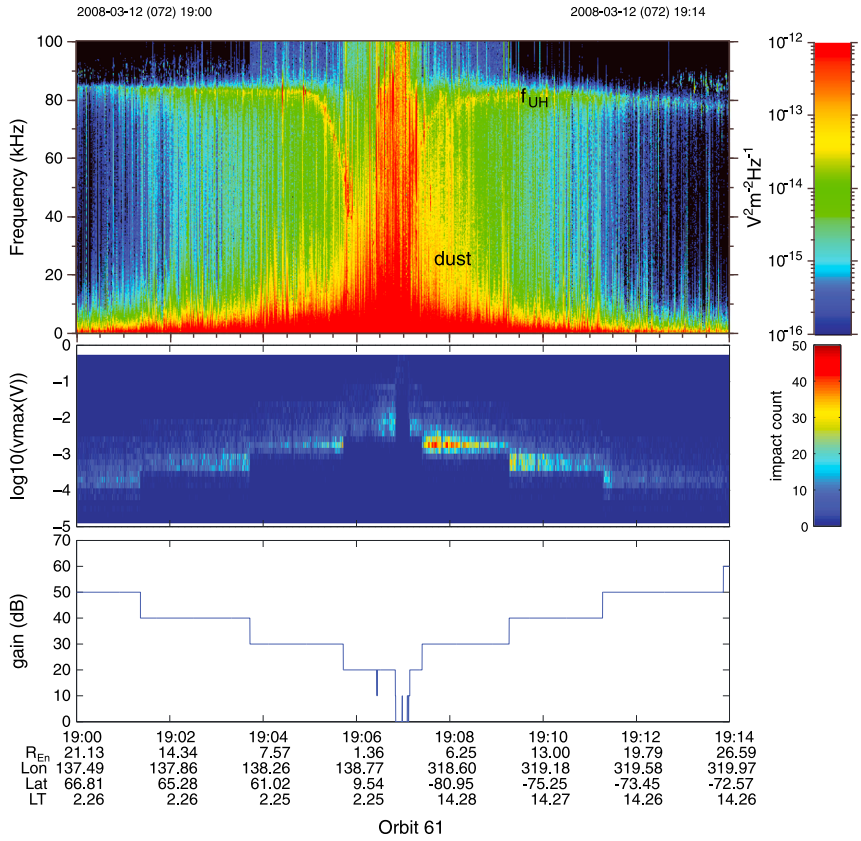

Figure 8. Dust impacts detected during the E3 flyby (12 March 2008) using dipole antenna. (top) WBR spectrogram shows wave power as a function of frequency and time. Dust impacts are identified as broadband bursts extending well above the local plasma frequency (indicated by the upper hybrid resonance). (middle) Number of dust impacts recorded in the WBR waveform snapshots as a function of peak voltage (base 10 logarithm) and time. (bottom) Variation of the gain of WBR during the E3 flyby.

moving window, because by the law of large numbers the average value from a large number of samples should be close to the expected value. When calculating the impact rates, the voltage/mass/size threshold should be carefully chosen, because the WBR is sensitive to different size ranges of dust grains at different gains. The threshold value is set at the median size of the impacts detected within the 5 s window. Under the assumption that the power law (exponent −4) size distribution extends to smaller sizes, we scale the impact rates to lower size thresholds in the same way as *Yaroshenko et al.* [2009] and *Shafiq et al.* [2011].

The impact rates for particles larger than a certain size threshold can be converted to dust density given the effective impact area and the ram velocity. The formula for the conversion is

$$n = R/(AU) \tag{6}$$

where R is the impact rate, U the ram velocity, and A the effective impact area for RPWS. In section 3, we derived the effective area of RPWS dust detection $A \sim 4\ \mathrm{m}^2$ based on the polarity ratio of the dust impacts and cross-sectional area of the electric monopole antenna. As discussed in section 4.2, the effective area for the dipole mode would be smaller due to the low sensitivity of some part of the spacecraft surface to the dust impacts. Because if a dust impact a location symmetric with respect to the two dipole antenna elements, the signal would be very small due to the common mode rejection. Therefore, we use $4\ \mathrm{m}^2$ as the effective area for the monopole mode and $1.5\ \mathrm{m}^2$ for the dipole mode.

4.5. Comparison With CDA Measurements

RPWS is not specially designed and calibrated for dust detection. So there are uncertainties in the mass conversion and the effective detection area of RPWS. In order to better infer the grain mass from the voltage pulse detected, we should cross-calibrate with the conventional dust detector, CDA. *Kurth et al.* [2006] made a

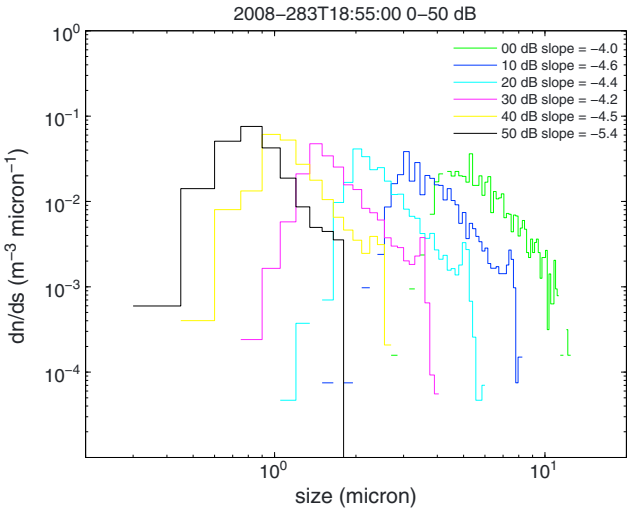

Figure 9. Differential size distribution of dust grains detected by RPWS WBR (dipole mode) during the E5 flyby. The voltage jump values are multiplied with a correction factor 40 to account for the lower charge antenna coupling efficiency in the dipole mode. Dust impacts are separated by the gain at which they are collected. The histograms of different gain levels displayed clear power law size distributions. The peaks near the larger end of the histograms are caused by underestimation of particle size due to saturation. The density ramp on the smaller end of the power law distributions are caused by the sensitivity limits of different gain levels of WBR.

preliminary attempt to cross calibrate the two instruments by comparing the RPWS impact rate to HRD counting rate during the E ring crossings. By setting the impact rates per unit area of RPWS (for a given size threshold) equal to that of the HRD, they scaled the effective area of RPWS dust detection from the effective area of HRD. $A \sim 0.5\ m^2$ effective impact area of RPWS was required for the consistency between the two instruments. This area is much smaller than the spacecraft cross-sectional area (~12 m^2), as originally assumed to be the impact area of RPWS during the SOI [*Wang et al*., 2006]. The large high-gain antenna, which was used to shield other instruments during the SOI, is made of material expected to have a very low (unknown) yield to dust impacts. The metallic part of the spacecraft and RPWS antennas is estimated to have a total projected surface area less than 1.5 m^2. One interpretation of the smaller effective area is that only direct impacts on the antenna can induce a voltage pulse in the WBR receiver, so the effective area is basically the projected area of the antennas [*Kurth et al*., 2006]. Alternatively, the WBR might have a larger mass threshold than previously estimated, which would lead to a smaller calibrated effective area [*Kurth et al*., 2006].

Since a new mass-to-charge relation is used in this study and there is less uncertainty in the monopole measurement, we compare the RPWS monopole data with CDA results. Figure 10 compares the dust densities measured by the monopole antenna of RPWS and the HRD of CDA during the ring plane crossing on DOY 248, 2005. The dust densities plotted are cumulative densities above selected size thresholds. The effective impact area used for the monopole mode is 4 m^2. Because the RPWS detection threshold changes during the ring plane crossing due to the gain change of the WBR, the RPWS dust density is scaled to that of the same threshold as CDA assuming a power law mass distribution with exponent −2. The comparison shows that the densities measured by the RPWS are about 3 times lower than those measured by the M sensor of HRD. The error bars of the HRD M sensor measurement, which are relatively large due to the low impact rate in this part of the E ring, are shown on top of the density curve. Nonetheless, the HRD data provide a baseline for the comparison with RPWS dust density measurement.

Several factors could have affected the RPWS dust density measurement. The mass of the dust particles detected by RPWS could be off by a factor of 10 (for instance, the charge yield or the charge collection efficiency could be overestimated). If so, the derived dust density above a certain mass threshold would correspond to that of a larger/smaller mass threshold, which would lead to an underestimation/overestimation of the density. As discussed before, the cumulative density is inverse proportional to the mass threshold according to the power law mass distribution (with a slope of −2) observed at Enceladus. For example, if we use a 10 times smaller charge yield coefficient or charge coupling coefficient, then the RPWS dust density will be 10 times higher for the same size threshold. The uncertainty in dust density associated with the RPWS effective impact area should be rather small compared to that with the mass uncertainty. To summarize, the uncertainties in the charge yield Q/m, the charge coupling coefficient α, and the effective impact area of the RPWS (relatively small) can all contribute to the uncertainty of the dust density measured by the RPWS. If the mass of the particles is an order of magnitude uncertain, the derived RPWS dust density

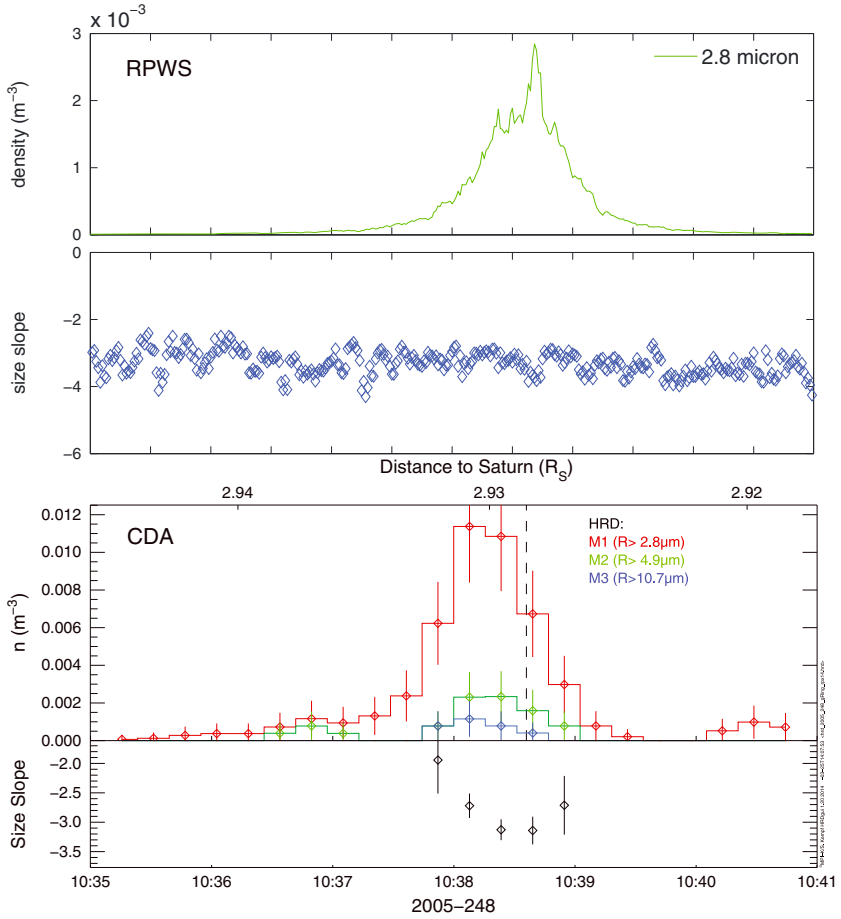

Figure 10. Dust density measured by the monopole antenna of (first and second panels) RPWS and (third and fourth panels) CDA HRD during the ring plane crossing on DOY 248, 2005. Figures 10 (second panel) and 10 (fourth panel) show the slope of the power law size distribution determined by fitting the cumulative density values with the size thresholds.

could be off by as much as factor of 10. The differences between the RPWS and CDA dust densities are well within this range. This uncertainty range is qualitatively similar to that concluded by *Kurth et al*. [2006].

Figure 11 compares the dust density measured by RPWS and CDA during the E7 flyby. During this flyby, the WBR was connected to the E_x dipole antenna. As discussed before, the effective impact area for the dipole mode is 1.5 m^2, smaller than the monopole mode due to the common mode rejection. The voltage pulses measured by the dipole antenna are multiplied by 40 to account for the lower sensitivity (compared to the monopole antenna) to dust impacts. The closest approach to Enceladus is marked by a red cross in the first panel. The black cross marks the closest approach to the center of the plume, which is approximated by the rotation axis of Enceladus. Similar spatial dust density variations (three peaks) were observed by the two instruments. The timings of the two latter peaks are quite consistent with the peaks measured in the water vapor and nanograin densities measured by the Ion and Neutral Mass Spectrometer and CAPS [*Dong*, 2014], which correspond to the water vapor jets associated with the dust jets in the Imaging Science Subsystem image [*Spitale and Porco*, 2007; *Hansen et al*., 2008]. The slopes of the size distribution inferred from the RPWS (Figure 11, second panel) and CDA (Figure 11, fourth panel) data are both around −4, which confirms that the size distribution of the dust particles is characterized by a power law distribution $dn/dr \propto r^{-4}$. Note that RPWS and CDA were sensitive to different size ranges of dust particles. During the plume crossing, the detection threshold of RPWS was shifted higher by the automatic gain control of the WBR. As a result, the mass threshold of RPWS is higher than that of CDA. Taking into account of the slower impact velocity, RPWS was sensitive to dust particles larger than about 10 μm near the center of the plume at 0 dB gain level. However, the dust density can be scaled to values corresponding to smaller size threshold assuming the power

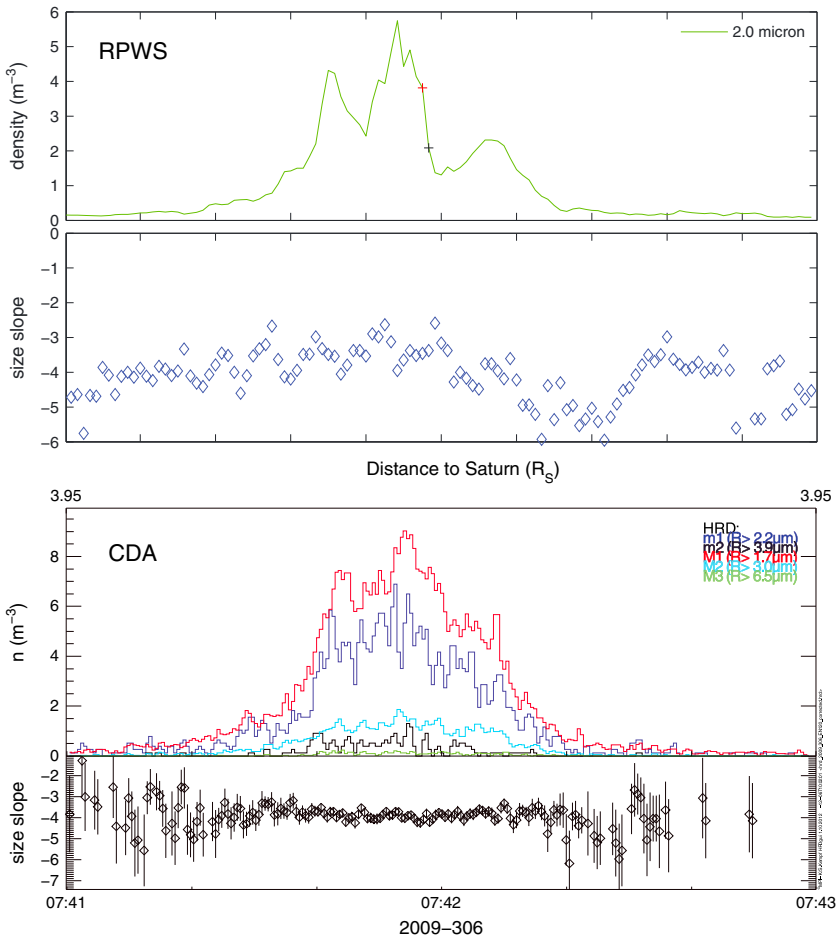

Figure 11. Dust density measured by the dipole antenna (voltage multiplied by 40) of (first and second panels) RPWS and (third and fourth panels) CDA HRD during the E7 flyby. The RPWS density is scaled from measurement with a higher size threshold (10 μm) assuming the power law size distribution with exponent −4 extends to smaller sizes. The red cross marks the closest approach to Enceladus. The black cross marks the closest approach to the center of the plume, approximated by the rotation axis of Enceladus. Figures 11 (second panel) and 11 (fourth panel) show the slope of the power law size distribution determined by fitting the cumulative density values with the size thresholds.

law size distribution extends to smaller sizes. The scaled RPWS peak dust density (6 m^{-3}) for a 2 μm threshold is within the uncertainty range when compared to the CDA peak density (6 m^{-3}) for the 2.2 μm threshold. Comparisons between RPWS and CDA data for different trajectories will help to better constrain the values of the impact charge yield, the charge coupling coefficient and the effective impact area.

5. Onboard Dust Detection

The wideband receiver also serves as the front end for the onboard dust detection function. The data compression processor is used to search the waveforms for the signature of dust impacts, based on the characteristics of the dust impacts observed by the Voyager plasma wave instrument [*Gurnett et al.*, 2004]. When WBR is not scheduled to capture high-resolution data, the onboard dust detection function is enabled, which captures the dust impact waveform as often as the program can process. The fastest rate of acquisition is about one snapshot every 4 or 5 s. The downlink of a detected dust waveform can take place as often as 450 s (approximately). The program updates the dust counts in the housekeeping data once every 64 s.

5.1. Onboard Dust Waveform Recorder

Figure 12 (left) shows a snapshot of waveform recorded by the onboard dust detection program. The WBR was connected to the E_w monopole antenna. The onboard dust detection algorithm counts dust impact

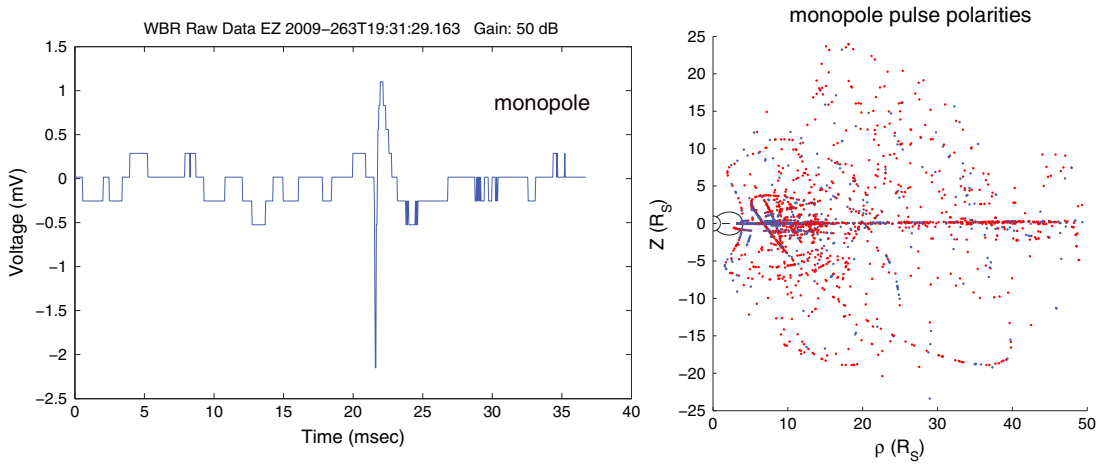

Figure 12. (left) Snapshot of dust impact waveform recorded by the onboard dust detection program with the E_w monopole antenna. (right) Polarities of voltage pulses induced by dust impacts recorded by the onboard program with the monopole antenna from 2004 to 2013. Red indicates positive voltage pulse; blue, negative. It can be inferred that the spacecraft potential is mostly negative near the equatorial plane inside ~10 R_S and mostly positive otherwise.

events that meet a rather stringent criterion, which requires that the jump in the digital counts due to the dust impact must exceed 64 counts within 3 samples. Thus, the effective threshold of the onboard algorithm, which varies with the gain level of the receiver, is higher than that applied to the ground analysis of wideband data [*Kurth et al*., 2006]. To save the memory space and transmitting bandwidth, the waveform data are decimated from 8 bits to 4 bits, causing the steps in the onboard waveform. Note the size of the voltage pulse in the waveform snapshots is proportional to the mass of the dust particles; thus, the onboard waveform data contain the statistical information of the mass/size of the particles in the magnetosphere of Saturn. However, proper assumptions on the impact speeds are needed when we try to derive the mass of the impacting particles from the voltages.

Another important piece of information that can be inferred from the onboard waveform data (monopole mode) is the sign of the spacecraft potential. As discussed earlier in this paper, when the wideband receiver is connected to a monopole antenna, the polarity of the voltage pulse induced by a dust impact depends on the impact location and the spacecraft potential. For example, if the spacecraft is negatively charged, most of the impact voltage pulses will be negative as the spacecraft body is the major impact target and charge collector. There are exceptions though. The opposite polarity is observed (less than 5%), when a dust particle impacts the monopole antenna. In Figure 12 (right), we plot the polarities of the dust impact voltage pulses recorded by the onboard dust detection program from 2004 to 2013 in a cylindrical projection. A red dot stands for a positive voltage pulse, and a blue dot stands for a negative voltage pulse. It is shown that near the equator and close to Saturn, mostly negative voltage pulses were observed. At higher latitudes and farther away from Saturn, mostly positive pulses were observed. This is consistent with the theory and observation that Cassini spacecraft is negatively charged in the cold dense plasma torus and positively charged in the hot tenuous plasma of the outer magnetosphere [*Wahlund et al*., 2005, 2009; *Morooka et al*., 2009, 2011; *Gustafsson and Wahlund*, 2010; *Hsu et al*., 2012, 2013]. Figure 12 (right) can be compared with Figure 1c of *Wahlund et al*. [2005], which shows that near the equatorial plane of Saturn, the Cassini spacecraft potential is negative inside 10 R_S and positive outside.

5.2. Onboard Dust Counter

Besides recording the waveforms of dust impacts, the on board program can also record the number of dust impacts within 64-second intervals. Also recorded are the number of data packets (1024 samples each) and the gain at which the dust impacts were recorded. Because the detection thresholds of different gains are different, we apply a correction factor $10^{(70\text{-dB})/20}$ to the dust counts recorded in different gains so that the resulting counts reflect the dust impacts that would have been detected if the detection thresholds were the same (as that of 70 dB, 0.4 μm at 10 km/s, 1.2 μm at 5 km/s). Then we divide the modified count by the total sampling time (36 μs × 1024 × number of packets) to get the impact rate. Figure 13 shows

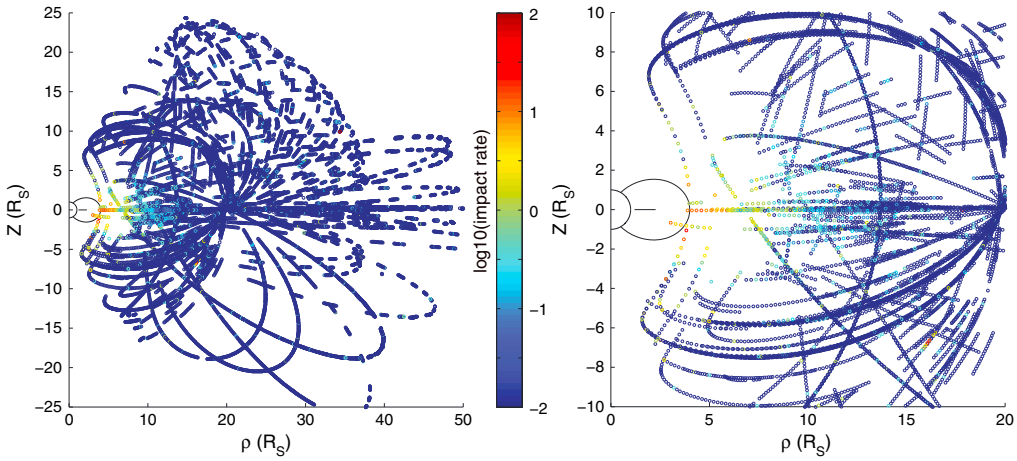

Figure 13. Logarithm (base 10) of dust impact rates recorded by the RPWS onboard dust detection program with the E_w monopole antenna.

the spatial distribution of the onboard dust impact rates (base 10 logarithm) in cylindrical coordinates. Only impact rates measured by the monopole antenna are plotted in this figure. It is clear that the highest impact rates are detected in the vicinity of the E-ring. It should be noted that during most of the Enceladus flybys and E-ring crossings, the onboard dust counter did not record data because the receiver was collecting data in the high-rate mode. So the order of magnitude difference in the impact rates should be higher than what is shown in Figure 13. The dust density above the 70 dB detection threshold can be calculated by $n = R/(AU)$, where R is the impact rate, A is the effective impact area (4 m^2), and U is the ram velocity. The ram velocity near the equator plane is approximated by subtracting the Keplerian velocity from the spacecraft velocity. But for higher-latitude orbits, we need some assumption on the trajectories of the dust particles to calculate the ram velocity.

6. Discussion

From the RPWS data collected in Saturn's magnetosphere, we can derive information about the dust population, e.g., size and spatial distribution, which will further our understanding of the role of dust particles in the overall dynamics of Saturn's magnetosphere. The parameters determined from our data, e.g., the size distribution and the cumulative density of the dust particles, are important input for the future modeling works.

In a dust-rich environment like Saturn's E ring and inside the plume of Enceladus, the spacecraft potential can be modified due to the relative motion of charged dusts and the spacecraft. *Hsu et al.* [2013] showed in their simulation that the spacecraft potential can become less negative due to the spacecraft collection of ions from the dust impact plasma cloud, which acts like a potential damper between the spacecraft and the ambient plasma. This potential damping process is closely related to the RPWS dust detection mechanism where the spacecraft potential is impulsively modified by the collection of charges generated by dust impacts.

We have shown the clear difference between the monopole and dipole measurement of dust impacts. The monopole antenna mode is more sensitive to dust impacts than the dipole antenna mode. The detection mechanism of the dipole mode is still controversial. Here we discuss several different scenarios.

1. The impact (on the spacecraft body) charges are collected by the spacecraft body, and the observed voltage pulses are caused by the imbalance in the common mode rejection. The weakness of this theory is that the polarity should always be the same.
2. Differential charging of the antennas by the expanding plasma cloud from a dust impact on the spacecraft body [*Gurnett et al.*, 1983, 1987; *Tsintikidis et al.*, 1994]. In this case, the signal level can depend on the location of dust impact relative to the antenna elements, which is affected by the spacecraft attitude. This scenario predicts fewer counts and smaller signals compared to the monopole measurement, which is consistent with the RPWS observation.
3. Direct impacts on the electric antenna, which collects impact charges [*Meyer-Vernet*, 1985; *Kurth et al.*, 2006]. There should be much fewer counts due to the smaller effective area of the antenna. The signal

level should be similar to the monopole measurement, but the observation shows that most of the impact signals observed on the dipole antenna are 30–50 times lower than on the monopole antenna. It is possible that larger pulses would be observed for occasional direct impacts on the antenna due to the more efficient charge collection of the antenna in this case. So some of the large pulses observed in the dipole mode might have been due to direct impacts on the antenna. But the probability of this happening is low due to the small cross-sectional area of the antenna compared to the spacecraft body. These direct impacts on the antenna would appear in the data as clipped pulses, the sizes of which are uncertain any way.

4. The ambipolar electric field in the expanding plasma cloud induces a voltage pulse on the electric antenna [*Tsurutani et al*., 2004]. The coupling efficiency of this mechanism is much smaller than the differential charging of antenna elements for the case of long dipole antenna [*Oberc*, 1996].
5. *Meyer-Vernet et al*. [2014] interpreted the dipole signal as the voltage jump on the antenna element induced by escaping charges. Their new mechanism is consistent with the amplitude and polarity of the voltage pulses observed on WIND when micron-sized dust particles impact the spacecraft [*Malaspina et al*., 2014].

Laboratory experiments have been funded to study the antenna signals induced by the dust impacts. The uncertainty in the dipole dust detection mechanism should be resolved by these experiments. Before that happens, we can multiply the dipole measurements with a voltage correction factor, thereby taking into account of the difference in the charge coupling efficiency in the two modes.

Recently a new coupling mechanism has been proposed by *Pantellini et al*. [2012b] and *Zaslavsky et al*. [2012] where the electric field in the expanding impact plasma cloud disrupts the plasma sheath around the electric field antenna resulting in a potential change of the antenna. Their theory applies to the fast nanograin impacts occurring in the low plasma density region where the monopole antenna is surrounded by a photoelectron sheath, which is often the case for STEREO. The voltage signal generated by a nanoparticle impact is very dependent on the impact geometry in this scenario.

The size calculation presented in the paper (section 4.3) involves uncertainty from different aspects. The yield constant in the mass-to-charge relation varies over an order of magnitude across different references [*Adams and Smith*, 1971; *Dietzel et al*., 1973; *Göller and Grün*, 1989]. The capacitance of the spacecraft body is estimated based on the dimension of the spacecraft, assuming Cassini is a sphere of 2 m radius. The uncertainty should be small compared to that of the impact charge yield constant. The exponent to the velocity is a function of impact speed and could range from 2.5 to 5.5 [*Dietzel et al*., 1973; *Krüger and Kissel*, 1984]. In this study, we keep the impact speed size independent, i.e., approximated by the difference between the spacecraft and Keplerian velocities. In reality, the speed of a dust particle depends on its charge-to-mass ratio due to the influence of Lorentz force [*Horanyi*, 1996]. Thus, the impact velocity is a function of grain size, which means the smaller particles have a higher impact speed than the larger ones. There are also uncertainties in the charge collection efficiency α, which we assume to be 0.5 for monopole measurement. In reality this number could depend on the surface material of the impact location. The charge-antenna coupling efficiency α for the dipole mode could be ~100 times smaller than that for the monopole mode [*Gurnett et al*., 1983, 1987; *Tsintikidis et al*., 1994]. Because the capacitance of the antenna is about half the capacitance of the spacecraft body, the difference in voltage response of the monopole and the dipole antennas to a dust impact is about 40 times. So the dipole voltage measurements are multiplied with a correction factor 40 to account for the difference. Taking all these factors into account, the mass of the particles inferred from the impact signals could be off by as much as one order of magnitude, which translates into a factor of 2.1 in the size uncertainty. The mass/size uncertainty and the uncertainty in the effective impact area (relatively small) both contribute to the uncertainty in the measured dust density (one order of magnitude). The discrepancies between the RPWS and CDA dust density measurements are well within the uncertainty range.

RPWS is sensitive to dust particles of a wide range of sizes, from a few microns to tens of microns. The sensitivity depends on the impact speed and dust density. As the spacecraft flew through the Enceladus plume, intense signals induced by frequent dust impacts drive the gain of the WBR down, increasing the size threshold of dust detection. Although the dust density level changes with location, the slope of the size distribution ($dn/dr \propto r^{-4}$, i.e., $dn/dm \propto m^{-2}$) remains around -4 as shown by the E5 flyby data.

Previously, optical observations and simulation works suggested a narrow distribution of particles near 1 μm for the E ring [*Showalter et al*., 1991; *Horanyi and Burns*, 1991]. This narrow size distribution is not given by the size distribution of the source, but a result of the dynamic filtering simulated by *Kempf et al*. [2010]. However, RPWS observations in the E ring show that this is not the case. The power law distribution extends from the detection threshold to the upper size limit of the WBR (determined by the dynamic range and gain level of the receiver) with no indication of a peak. The roll-offs near the detection thresholds in these size distributions are caused by the reduced sensitivity of the detection algorithm to small impact signals. In Figure 7, the peaks at the upper size limit of the histograms indicate clipped signals caused by dust particles larger than the upper size limits of the corresponding gain levels. This indicates that the power law size distribution applies to a wider-size range than the instrument limit.

Schmidt et al. [2008], through thermal dynamic modeling of grain formation in the vents on Enceladus, showed that the dust particle size distribution can be characterized as a power law distribution. The modeled particle size distribution generally agrees with the CDA HRD measurement during the E2 flyby. *Hedman et al*. [2009] derived the spatially resolved particle density on the Enceladus plume based on the observation by the Visual and Infrared Mapping Spectrometer (VIMS) instrument of Cassini. The density profile of the plume can in turn be converted into the velocity distribution of particles launched from the surface. The optical data indicate that larger particles are launched from the moon's south pole at lower velocities than smaller particles, which would lead to an altitude-dependent size distribution for the particles inside the plume. However, the size distribution slopes measured by RPWS during the E5 flyby (Figure 9) remained around −4 as the spacecraft crossed through the plume with a high inclination orbit (increasing altitude). The size slope measured by RPWS is larger for the E9 flyby, around −5, when Cassini flew across the base of the plume at a much lower altitude. Also, RPWS did not observe the strong depletion of dust particles larger than 4 μm relative to the power law distribution inside the Enceladus plume, as indicated by the optical result of VIMS [*Hedman* et al., 2009].

Hill et al. [2012] based on CAPS measurements of nanoparticles (~0.5–2.0 nm) in the Enceladus plume inferred that nanoparticles (2–20 nm) dominate in both the charge and the number densities. Although the 2–500 nm particles are not measured by any instrument onboard Cassini, one can assume that the power law distribution applies to these particles because no sign of peaking in the size distribution is observed around the detection threshold of RPWS. *Farrell et al*. [2012] compared the measurements between ELS, CDA, and RPWS with the constraint of the total charge implied by the Langmuir probe and confirmed the power law distribution. *Dong and Hill* [2013] proposed a composite size distribution for the ice grains in the Enceladus plume combining the CAPS nanograin and the CDA/RPWS dust size distributions. The model size distribution peaks at a few nanometers and asymptotically approaches power law size distribution when the size increases toward 1 μm. These studies confirmed the predictions by *Morooka et al*. [2011] and *Shafiq et al*. [2011] that most electrons are attached to the nanometer and submicron grains, as inferred from Langmuir probe electron and ion density measurements.

7. Conclusion

As Cassini orbits Saturn, the RPWS/WBR can detect micron to tens of micron-sized dust particles via the voltage pulses induced by dust impacts. The WBR provides continuous measurements of the impact rates, number densities, and size distributions of dust grains. The range of detectable sizes depends on impact velocity, dust flux, and the gain of the receiver. The size distribution of the dust particles near Saturn can be characterized as a power law $dn/dr \propto r^{\mu}$, where $\mu \sim -4$, n is the density, and r is the particle size. No peak is observed in the size distribution, contrary to the narrow size distribution shown by optical data and simulations. Comparison of the RPWS data with the CDA results shows that similar density profiles and size distributions are observed by the two instruments. The differences in dust densities measured by the two instruments are within the uncertainty range estimated for the RPWS dust density measurements. Because the RPWS dust detection is not reliant on spacecraft attitude, virtually continuous measurement of the dust properties is carried out by the onboard program. The RPWS onboard dust detection data provide the possibility to map the dust density distribution over Saturn's magnetosphere. The polarities of the dust impact voltage pulses measured by the monopole antenna can be used to statistically infer the charge state of the spacecraft, which complements the Langmuir probe measurement.

Acknowledgments
This research was supported by NASA through contract 1415150 with the Jet Propulsion Laboratory. The authors thank Sebastian Pawlinka and Andrew Collette for providing the results of the impact charge yield experiment and Michiko Morooka for providing the LP spacecraft potential data. S.Y. thanks Yaxue Dong and Donald Kirchner for helpful discussions. The data used in this study are available through the Planetary Data System or from the authors.

Michael Balikhin thanks the reviewers for their assistance in evaluating this paper.

References

Adams, N. G., and D. Smith (1971), Studies of microparticle impact phenomena leading to development of a highly sensitive micrometeoroid detector, *Planet. Space Sci.*, *19*(2), 195–204, doi:10.1016/0032-0633(71)90199-1.

Aubier, M. G., N. Meyer-Vernet, and B. M. Pedersen (1983), Shot noise from grain and particle impacts in Saturn's ring plane, *Geophys. Res. Lett.*, *10*, 5–8, doi:10.1029/GL010i001p00005.

Dietzel, H., G. Eichhorn, H. Fechtig, E. Grun, H. J. Hoffmann, and J. Kissel (1973), HEOS 2 and HELIOS micrometeoroid experiments, *J. Phys. E Sci. Instrum.*, *6*(3), 209–217, doi:10.1088/0022-3735/6/3/008.

Dong, Y. (2014), The water vapor and dust plumes of Enceladus, PhD thesis, Rice Univ., Houston, Tex.

Dong, Y., and T. Hill (2013), A study of the charged ice grains in the Enceladus plume with a composite size distribution, Abstract #P32B-04 presented at 2013 Fall meeting, AGU, San Francisco, Calif., 9–13 Dec.

Dong, Y., T. W. Hill, B. D. Teolis, B. A. Magee, and J. H. Waite (2011), The water vapor plumes of Enceladus, *J. Geophys. Res.*, *116*, A10204, doi:10.1029/2011JA016693.

Dougherty, M. K., K. K. Khurana, F. M. Neubauer, C. T. Russell, J. Saur, J. S. Leisner, and M. Burton (2006), Identification of a dynamic atmosphere at Enceladus with the Cassini magnetometer, *Science*, *311*, 1406–1409.

Farrell, W. M., W. S. Kurth, D. A. Gurnett, R. E. Johnson, M. L. Kaiser, J.-E. Wahlund, and J. H. Waite Jr. (2009), Electron density dropout near Enceladus in the context of water-vapor and water-ice, *Geophys. Res. Lett.*, *36*, L10203, doi:10.1029/2008GL037108.

Farrell, W. M., W. S. Kurth, R. L. Tokar, J. E. Wahlund, D. A. Gurnett, Z. Wang, R. J. MacDowall, M. W. Morooka, R. E. Johnson, and J. H. Waite (2010), Modification of the plasma in the near-vicinity of Enceladus by the enveloping dust, *Geophys. Res. Lett.*, *37*, L20202, doi:10.1029/2010GL044768.

Göller, J. R., and E. Grün (1989), Calibration of the Galileo Ulysses dust detectors with different projectile materials and at varying impact angles, *Planet. Space Sci.*, *37*(10), 1197–1206, doi:10.1016/0032-0633(89)90014-7.

Grün, E., H. A. Zook, H. Fechtig, and R. H. Giese (1985), Collisional balance of the meteoritic complex, *Icarus*, *62*(2), 244–272, doi:10.1016/0019-1035(85)90121-6.

Gurnett, D. A. (1998), Principles of space plasma wave instrument design, in *Measurement Techniques for Space Plasmas*, *AGU Monogr.*, vol. 103, edited by R. Pfaff, J. Borovsky, and D. Young, pp. 121–136, AGU, Washington, D. C.

Gurnett, D. A., E. Grün, D. Gallagher, W. S. Kurth, and F. L. Scarf (1983), Micron-sized particles detected near Saturn by the Voyager plasma wave instrument, *Icarus*, *53*, 236–254.

Gurnett, D. A., W. S. Kurth, F. L. Scarf, J. A. Burns, J. N. Cuzzi, and E. Grün (1987), Micron-sized particle impacts detected near Uranus by the Voyager 2 plasma wave instrument, *J. Geophys. Res.*, *92*, 14,959–14,968, doi:10.1029/JA092iA13p14959.

Gurnett, D. A., W. S. Kurth, L. J. Granroth, S. C. Allendorf, and R. L. Poynter (1991), Micron-sized particles detected near Neptune by the Voyager 2 plasma wave instrument, *J. Geophys. Res.*, *96*, 19,177–19,186, doi:10.1029/91JA01270.

Gurnett, D. A., et al. (2004), The Cassini radio and plasma wave science investigation, *Space Sci. Rev.*, *114*, 395–463.

Gustafsson, G., and J. E. Wahlund (2010), Electron temperatures in Saturn's plasma disc, *Planet. Space Sci.*, *58*(7–8), 1018–1025, doi:10.1016/j.pss.2010.03.007.

Hansen, C. J., L. W. Esposito, A. I. F. Stewart, B. Meinke, B. Wallis, J. E. Colwell, A. R. Hendrix, K. Larsen, W. Pryor, and F. Tian (2008), Water vapour jets inside the plume of gas leaving Enceladus, *Nature*, *456*(7221), 477–479, doi:10.1038/nature07542.

Hedman, M. M., P. D. Nicholson, M. R. Showalter, R. H. Brown, B. J. Buratti, and R. N. Clark (2009), Spectral observation of the enceladus plume with Cassini-Vims, *Astrophysical Journal*, *693*(2), 1749–1762, doi:10.1088/0004-637x/693/2/1749.

Hill, T. W., et al. (2012), Charged nanograins in the Enceladus plume, *J. Geophys. Res.*, *117*, A05209, doi:10.1029/2011JA017218.

Horanyi, M. (1996), Charged dust dynamics in the solar system, *Annu. Rev. Astron. Astrophys.*, *34*, 383–418.

Horanyi, M., and J. A. Burns (1991), Charged dust dynamics—Orbital resonance due to planetary shadows, *J. Geophys. Res.*, *96*, 19,283–19,289, doi:10.1029/91JA01982.

Horanyi, M., A. Juhasz, and G. E. Morfill (2008), Large-scale structure of Saturn's E-ring, *Geophys. Res. Lett.*, *35*, L04203, doi:10.1029/2007GL032726.

Hsu, H.-W., M. Horányi, S. Kempf, and E. Grün (2012), Spacecraft charging near Enceladus, *Geophys. Res. Lett.*, *39*, L06108, doi:10.1029/2012GL050999.

Hsu, H.-W., M. Horanyi, and S. Kempf (2013), Dust and spacecraft charging in Saturn's E ring, *Earth Planets Space*, *65*, 149–156.

Humes, D. H., R. L. O'Neal, W. H. Kinard, and J. M. Alvarez (1980), Impact of Saturn ring particles on Pioneer 11, *Science*, *207*, 443–444.

Jones, G. H., et al. (2009), Fine jet structure of electrically charged grains in Enceladus's plume, *Geophys. Res. Lett.*, *36*, L16204, doi:10.1029/2009GL038284.

Juhasz, A., and M. Horanyi (2002), Saturn's E ring: A dynamical approach, *J. Geophys. Res.*, *107*(A6), 1066, doi:10.1029/2001JA000182.

Juhasz, A., M. Horanyi, and G. E. Morfill (2007), Signatures of Enceladus in Saturn's E ring, *Geophys. Res. Lett.*, *34*, L09104, doi:10.1029/2006GL029120.

Kempf, S., U. Beckmann, G. Klostermeyer, F. Postberg, R. Srama, T. Economou, J. Schmidt, F. M. Spahn, and E. Grün (2008), The E ring in the vicinity of Enceladus I. Spatial distribution and properties of the ring particles, *Icarus*, *193*, 420–437.

Kempf, S., U. Beckmann, and J. Schmidt (2010), How the Enceladus dust plume feeds Saturn's E ring, *Icarus*, *206*, 446–457.

Krüger, F. R., and J. Kissel (1984), Experimental investigations on ion emission with dust impact on solid surfaces, in *Proceedings of the GIOTTO Plasma Environment Working Group Meeting, 10–12 April 1984, Bern, Switzerland*, ESA SP-224, pp. 43–48.

Kurth, W. S., T. F. Averkamp, D. A. Gurnett, and Z. Wang (2006), Cassini RPWS observations of dust in Saturn's E ring, *Planet. Space Sci.*, *54*, 988–998.

Lee, N., et al. (2012), Measurements of freely-expanding plasma from hypervelocity impacts, *Int. J. Impact Eng.*, *44*, 40–49.

Lee, N., S. Close, A. Goel, D. Lauben, I. Linscott, T. Johnson, D. Strauss, S. Bugiel, A. Mocker, and R. Srama (2013), Theory and experiments characterizing hypervelocity impact plasmas on biased spacecraft materials, *Phys. Plasmas*, *20*(3), 032901, doi:10.1063/1.4794331.

Malaspina, D. M., M. Horanyi, A. Zaslavsky, K. Goetz, L. B. Wilson, and K. Kersten (2014), Interplanetary and interstellar dust observed by the Wind WAVES electric field instrument, *Geophys. Res. Lett.*, *41*, 266–272, doi:10.1002/2013GL058786.

McBride, N., and J. A. M. McDonnell (1999), Meteoroid impacts on spacecraft: Sporadics, streams, and the 1999 Leonids, *Planet. Space Sci.*, *47*, 1005–1013.

Meyer-Vernet, N. (1985), Comet Giacobini-Zinner diagnosis from radio measurements, *Adv. Space Res.*, *5*, 37–46.

Meyer-Vernet, N., P. Couturier, S. Hoang, C. Perche, J. L. Steinberg, J. Fainberg, and C. Meetre (1986), Plasma diagnosis from thermal noise and limits on dust flux or mass in comet Giacobini-Zinner, *Science*, *232*(4748), 370–374, doi:10.1126/science.232.4748.370.

Meyer-Vernet, N., A. Lecacheux, and B. M. Pedersen (1996), Constraints on Saturn's E ring from the Voyager 1 radio astronomy instrument, *Icarus*, *123*, 113–129.

Meyer-Vernet, N., A. Lecacheux, M. L. Kaiser, and D. A. Gurnett (2009), Detecting nanoparticles at the radio frequencies: Jovian dust stream impacts on Cassini/RPWS, *Geophys. Res. Lett.*, *36*, L03103, doi:10.1029/2008GL036752.

Meyer-Vernet, N., M. Moncuquet, K. Issautier, and A. Lecacheux (2014), The importance of monopole antennas for dust observations: Why Wind/WAVES does not detect nanodust, *Geophys. Res. Lett.*, *41*, 2716–2720, doi:10.1002/2014GL059988.

Morooka, M. W., et al. (2009), The electron density of Saturn's magnetosphere, *Annales Geophysicae*, *2*(7), 2971–2991.

Morooka, M. W., J.-E. Wahlund, A. I. Eriksson, W. M. Farrell, D. A. Gurnett, W. S. Kurth, A. M. Persoon, M. Shafiq, M. André, and M. Holmberg (2011), Dusty plasma in the vicinity of Enceladus, *J. Geophys. Res.*, *116*, A12221, doi:10.1029/2011JA017038.

Nicholson, P. D., M. R. Showalter, and L. Dones (1996), Observations of Saturn's ring-plane crossing in August and November, *Science*, *272*, 509–516.

Oberc, P. (1996), Electric antenna as a dust detector, *Adv. Space Res.*, *17*, 105–110.

Omidi, N., R. L. Taker, T. Averkamp, D. A. Gurnett, W. S. Kurth, and Z. Wang (2012), Flow stagnation at Enceladus: The effects of neutral gas and charged dust, *J. Geophys. Res.*, *117*, A06230, doi:10.1029/2011JA017488.

Pantellini, F., S. Landi, A. Zaslavsky, and N. Meyer-Vernet (2012a), On the unconstrained expansion of a spherical plasma cloud turning collisionless: Case of a cloud generated by a nanometre dust grain impact on an uncharged target in space, *Plasma Phys. Controlled Fusion*, *54*(4), 045005, doi:10.1088/0741-3335/54/4/045005.

Pantellini, F., S. Belheouane, N. Meyer-Vernet, and A. Zaslavsky (2012b), Nano dust impacts on spacecraft and boom antenna charging, *Astrophys. Space Sci.*, *341*, 309–314.

Pedersen, B. M., N. Meyervernet, M. G. Aubier, and P. Zarka (1991), Dust distribution around Neptune—Grain impacts near the ring plane measured by the Voyager Planetary Radio Astronomy experiment, *J. Geophys. Res.*, *96*, 19,187–19,196, doi:10.1029/91JA01601.

Porco, C. C., et al. (2006), Cassini observes the active south pole of Enceladus, *Science*, *311*, 1393–1401.

Saur, J., N. Schilling, F. M. Neubauer, D. F. Strobel, S. Simon, M. K. Dougherty, C. T. Russell, and R. T. Pappalardo (2008), Evidence for temporal variability of Enceladus' gas jets: Modeling of Cassini observations, *Geophys. Res. Lett.*, *35*, L20105, doi:10.1029/2008GL035811.

Scarf, F. L., D. A. Gurnett, W. S. Kurth, and R. L. Poynter (1982), Voyager 2 plasma wave observations at Saturn, *Science*, *215*, 587–594.

Schmidt, J., N. Brilliantov, F. Spahn, and S. Kempf (2008), Slow dust in Enceladus' plume from condensation and wall collisions in tiger stripe fractures, *Nature*, *451*(7179), 685–688, doi:10.1038/nature06491.

Shafiq, M., J.-E. Wahlund, M. W. Morooka, W. S. Kurth, and W. M. Farrell (2011), Characteristics of the dust-plasma interaction near Enceladus' south pole, *Planet. Space Sci.*, *59*, 17–25.

Sheehan, D. P., C. A. Casey, and L. T. Volt (1995), Interaction of an expanding plasma cloud with a simple antenna—Application to anomalous voltage signals observed by Voyager-1, Voyager-2, ICE, and VEGA spacecraft, *J. Geophys. Res.*, *100*, 19,805–19,808, doi:10.1029/95JA01986.

Showalter, M. R., J. N. Cuzzi, and S. M. Larson (1991), Structure and particle properties of Saturn's E ring, *Icarus*, *94*, 451–473.

Sittler, E. C., et al. (2006), Cassini observations of Saturn's inner plasmasphere: Saturn orbit insertion results, *Planet. Space Sci.*, *54*(12), 1197–1210, doi:10.1016/j.pss.2006.05.038.

Smith, H. T., R. E. Johnson, M. E. Perry, D. G. Mitchell, R. L. McNutt, and D. T. Yound (2010), Enceladus plume variability and the neutral gas densities in Saturn's magnetosphere, *J. Geophys. Res.*, *115*, A10252, doi:10.1029/2009JA015184.

Spahn, F., et al. (2006), Cassini dust measurements at Enceladus and implications for the origin of the E ring, *Science*, *311*, 1416–1418.

Spitale, J. N., and C. C. Porco (2007), Association of the jets of Enceladus with the warmest regions on its south-polar fractures, *Nature*, *449*(7163), 695–697, doi:10.1038/nature06217.

Srama, R., et al. (2004), The Cassini cosmic dust analyzer, *Space Sci. Rev.*, *114*, 465–518.

Srama, R., et al. (2006), In situ dust measurements in the inner Saturnian system, *Planet. Space Sci.*, *54*, 967–987.

Timmermann, R., and E. Grün (1991), Plasma emission from high velocity impacts of microparticles onto water ice, in *Origin and Evolution of Interplanetary Dust*, edited by A. C. Levasseur-Regourd and H. Hasegawa, pp. 375–378, Kluwer Academic, Dordrecht, Netherlands.

Tsintikidis, D., D. A. Gurnett, L. J. Granroth, S. C. Allendorf, and W. S. Kurth (1994), A revised analysis of micron-sized particle detected near Saturn by the Voyager 2 plasma wave instrument, *J. Geophys. Res.*, *99*, 2261–2270, doi:10.1029/93JA02906.

Tsintikidis, D., W. S. Kurth, D. A. Gurnett, and D. D. Barbosa (1995), A study of dust in the vicinity of Dione using the Voyager 1 plasma wave instrument, *J. Geophys. Res.*, *100*, 1811–1822, doi:10.1029/94JA02357.

Tsurutani, B. T., D. R. Clay, L. D. Zhang, B. Dasgupta, D. Brinza, M. Henry, J. K. Arballo, S. Moses, and A. Mendis (2004), Plasma clouds associated with Comet P Borrelly dust impacts, *Icarus*, *167*(1), 89–99, doi:10.1016/j.icarus.2003.08.021.

Wahlund, J.-E., et al. (2005), The inner magnetosphere of Saturn: Cassini RPWS cold plasma result from the first encounter, *Geophys. Res. Lett.*, *32*, L20S09, doi:10.1029/2005GL022699.

Wahlund, J.-E., et al. (2009), Detection of dusty plasma near the E-ring of Saturn, *Planet. Space Sci.*, *57*, 1795–1806.

Waite, J. H., et al. (2006), Cassini ion and neutral mass spectrometer: Enceladus plume composition and structure, *Science*, *311*, 1419–1422.

Wang, Z., D. A. Gurnett, T. F. Averkamp, A. M. Persoon, and W. S. Kurth (2006), Characteristics of dust particles detected near Saturn's ring plane, *Planet. Space Sci.*, *54*, 957–966.

Warwick, J. W., et al. (1982), Planetary radio astronomy observations from Voyager 2 near Saturn, *Science*, *215*, 582–587.

Yaroshenko, V. V., S. Ratynskaia, J. Olson, N. Brenning, J.-E. Wahlund, M. Morooka, W. S. Kurth, D. A. Gurnett, and G. E. Morfill (2009), Characteristics of charged dust inferred from the Cassini RPWS measurements in the vicinity of Enceladus, *Planet. Space Sci.*, *57*, 1807–1812.

Zaslavsky, A., et al. (2012), Interplanetary dust detection by radio antennas: Mass calibration and fluxes measured by STEREO/WAVES, *J. Geophys. Res.*, *117*, A05102, doi:10.1029/2011JA017480.